ISSN 1674-1056
http://cpb.iphy.ac.cn
http://iopscience.iop.org/cpb
中国物理 B
Chinese Physics
中国物理 Chinese Physics B

Polarized photoluminescence spectroscopy in WS_2, WSe_2 atomic layers and heterostructures by cylindrical vector beams

Lijun Wu(吴莉君), Cuihuan Ge(葛翠环), Kai Braun, Mai He(贺迈), Siman Liu(刘思嫚), Qingjun Tong(童庆军), Xiao Wang(王笑), and Anlian Pan(潘安练)

Citation: Chin. Phys. B, 2021, 30 (**8**): 087802. DOI: 10.1088/1674-1056/abf3b6
Journal homepage: http://cpb.iphy.ac.cn; http://iopscience.iop.org/cpb

What follows is a list of articles you may be interested in

Linear and nonlinear optical response of g-C_3N_4-based quantum dots

Jing-Zhi Zhang(张竞之) and Hong Zhang(张红)
Chin. Phys. B, 2021, 30 (**7**): 077802. DOI: 10.1088/1674-1056/abec2f

Low-dimensional phases engineering for improving the emission efficiency and stability of quasi-2D perovskite films

Yue Wang(王月), Zhuang-Zhuang Ma(马壮壮), Ying Li(李营), Fei Zhang(张飞), Xu Chen(陈旭), and Zhi-Feng Shi(史志锋)
Chin. Phys. B, 2021, 30 (**6**): 067802. DOI: 10.1088/1674-1056/abe92b

Thermally induced band hybridization in bilayer-bilayer MoS_2/WS_2 heterostructure

Yanchong Zhao(赵岩翀), Tao Bo(薄涛), Luojun Du(杜罗军), Jinpeng Tian(田金朋), Xiaomei Li(李晓梅), Kenji Watanabe, Takashi Taniguchi, Rong Yang(杨蓉), Dongxia Shi(时东霞), Sheng Meng(孟胜), Wei Yang(杨威), and Guangyu Zhang(张广宇)
Chin. Phys. B, 2021, 30 (**5**): 057801. DOI: 10.1088/1674-1056/abeee3

Optical polarization characteristics for AlGaN-based light-emitting diodes with AlGaN multilayer structure as well layer

Lu Xue(薛露), Yi Li(李毅), Mei Ge(葛梅), Mei-Yu Wang(王美玉), and You-Hua Zhu(朱友华)
Chin. Phys. B, 2021, 30 (**4**): 047802. DOI: 10.1088/1674-1056/abcf3f

Optical polarization response at gold nanosheet edges probed by scanning near-field optical microscopy

Zhuan-Fang Bi(毕篆芳), Mu Yang(杨沐), Guang-Yi Shang(商广义)
Chin. Phys. B, 2018, 27 (**8**): 087801. DOI: 10.1088/1674-1056/27/8/087801

SPECIAL TOPIC — Optical field manipulation

Polarized photoluminescence spectroscopy in WS_2, WSe_2 atomic layers and heterostructures by cylindrical vector beams*

Lijun Wu(吴莉君)[1], Cuihuan Ge(葛翠环)[1], Kai Braun[1,2], Mai He(贺迈)[1], Siman Liu(刘思嫚)[1], Qingjun Tong(童庆军)[1], Xiao Wang(王笑)[1,†], and Anlian Pan(潘安练)[3]

[1] *Key Laboratory for Micro-Nano Physics and Technology of Hunan Province, School of Physics and Electronics, Hunan University, Changsha, Hunan* 410082, *China*

[2] *Institute of Physical and Theoretical Chemistry and LISA+, University of Tübingen, Auf der Morgenstelle* 18, 72076, *Tübingen, Germany*

[3] *College of Materials Science and Engineering, Hunan University, Changsha, Hunan* 410082, *China*

(Received 4 February 2021; revised manuscript received 20 March 2021; accepted manuscript online 31 March 2021)

Due to the large exciton binding energy, two-dimensional (2D) transition metal dichalcogenides (TMDCs) provide an ideal platform for studying excitonic states and related photonics and optoelectronics. Polarization states lead to distinct light–matter interactions which are of great importance for device applications. In this work, we study polarized photoluminescence spectra from intralayer exciton and indirect exciton in WS_2 and WSe_2 atomic layers, and interlayer exciton in WS_2/WSe_2 heterostructures by radially and azimuthally polarized cylindrical vector laser beams. We demonstrated the same in-plane and out-of-plane polarization behavior from the intralayer and indirect exciton. Moreover, with these two laser modes, we obtained interlayer exciton in WS_2/WSe_2 heterostructures with stronger out-of-plane polarization, due to the formation of vertical electric dipole moment.

Keywords: two-dimensional transition metal dichalcogenides, optical polarization, interlayer exciton, cylindrical vector beams

PACS: 78.67.−n, 42.25.Ja, 71.35.−y **DOI:** 10.1088/1674-1056/abf3b6

1. Introduction

Two-dimensional transition metal dichalcogenides (TMDCs) such as MoS_2, $MoSe_2$, WS_2, and WSe_2 are emerging low-dimensional semiconductor materials, which have attracted much attention due to their intriguing optoelectronic properties as well as practical spin, valley related photonic, and optoelectronic applications.[1–8] Owing to the two-dimensional nature and the reduced dielectric screening effect, TMDCs atomic layers exhibit up to hundred meV large exciton binding energy,[9] providing an ideal platform for studying excitonic states and related devices.[10–14] The so-called A-, B-excitons in TMDCs atomic layers are formed at the K/K' point in the Brillouin region,[15] which are also named as intralayer excitons, since the electrons and holes are spatially located at the same layer of the TMDCs. Increasing the layer number of TMDCs from monolayer to bilayer and multi-layers, the interlayer coupling affects the band structure, leading to the transition from direct to indirect bandgap semiconductors with the appearance of indirect excitons.[16,17] Besides, interlayer excitons consisting of electrons and holes in different layers can also be formed in TMDCs bilayers[18] due to the hole delocalization over the bilayer.[19] However, this requires a special treatment during the sample preparation. The formation of 2D Van der Waals heterostructures[20,21] combines the advantages of individual materials and offers new means to manipulate physical properties.[22–25] In addition, interlayer excitons in TMDCs heterostructures, which are formed with electrons and holes located in different materials and layers,[21] can be obtained and the energy can be tuned by choosing different 2D martials.[26] Interlayer excitons play a key role in the application of heterojunctions due to the long lifetime, valley related properties, and tunability with an applied electric field.[11,27–30]

Due to the distinct formation mechanisms, the intra- and interlayer excitons compose different electric dipole moments, which lead to the different light–matter interaction conditions,[31] such as the dominated in-plane or out-of-plane optical response. Therefore, a detailed understanding of the interaction between the electric field of light and the effective dipole moment of intra- and interlayer excitons as well as the indirect exciton, is of great significance for fundamental research and practical device application.[32] However, the normally used linear polarized laser beam in optical microscopy creates only in-plane electric fields at the focus, which limits the study of different excitation conditions.

The introduction of cylindrical vector beams (CVBs) such as radially or azimuthally polarized laser beams[33,34] can

*Project supported by the National Natural Science Foundation of China (Grant Nos. 91850116, 51772084, 52022029, and U19A2090), Hunan Provincial Natural Science Foundation of China (Grant Nos. 2018RS3051 and 2018WK4004), and the Key Program of the Hunan Provincial Science and Technology Department, China (Grant No. 2019XK2001).

†Corresponding author. E-mail: xiao_wang@hnu.edu.cn

© 2021 Chinese Physical Society and IOP Publishing Ltd

overcome this problem. Focused by a high numerical aperture (NA) objective, the azimuthally polarized laser beam creates only in-plane (transverse) electric fields, while out-of-plane (longitudinal) electric field component can be obtained with the radially polarized laser beam.[34] CVBs have been utilized to study linear and nonlinear optical properties of various materials, such as single molecules,[35] molecular terraces,[36] semiconductor nanowires,[37,38] and metal nanostructures.[39] With these two different CVBs, we can realize the in-plane and out-of-plane optical excitation configurations in TMDCs.

In this work, we study the polarized PL spectroscopy of WS_2, WSe_2, and bilayer WS_2/WSe_2 heterostructures using radially and azimuthally polarized laser beams. Excitation power dependent polarized PL spectra were collected from WS_2 and WSe_2 with different layer thicknesses. We observed strong PL emission with the in-plane electric field excitation (azimuthal mode). Furthermore, we found that the A-exciton and indirect bandgap transition PL peaks show the same in-plane and out-of-plane polarizations. We further studied the PL of interlayer excitons in WS_2/WSe_2 heterostructures, which show much stronger PL emission with the out-of-plane excitation, indicating the different electric dipole moments compared with the intralayer excitons. The use of CVBs in this work can be applied to other 2D TMDCs semiconductors and heterostructures to fulfill the different optical excitation conditions.

2. Materials and methods

Mono- (1L), bi- (2L), tri- (3L), and quad-layer (4L) WS_2 and WSe_2 were prepared by mechanical exfoliation from the bulk materials (purchased from HQ Graphene) and were transferred to transparent glass slides (22×22 mm) for optical polarization measurements. Bilayer WS_2/WSe_2 heterostructures were obtained by manually stacking the corresponding exfoliated monolayers using the standard dry transfer and stacking technique.[4] The formed heterostructures were further annealed in vacuum at 150 °C for two hours to optimize the interface of the heterostructures.

For optical polarization measurements, a linearly polarized 532 nm continuous wave semiconductor laser was converted to a radially or an azimuthally polarized cylindrical vector beam through a commercial liquid crystal (LC) polarization converter (ARCoptix) (supporting information Fig. S1). In the optical path, a pinhole (diameter = 100 μm) was used to filter out the higher-order modes of the laser beam. The created radial and azimuthal polarizations can be distinguished by monitoring the orientation of the beam patterns after passing a rotating linear polarizer (supporting information Fig. S1(d)). An inverted confocal microscope (OLYMPUS IX73) equipped with an oil-immersion objective (NA = 1.4) was used to focus the cylindrical vector beams onto the sample surface. A spectrometer (HORIBA iHR320) with a liquid-nitrogen cooled CCD (Symphony II) was used to collect the emitted optical signals.

Due to the different polarizations of the excitation laser beams, we can obtain distinct electric field distributions at the focus. For the radially polarized laser beam, as shown by the theoretically calculated field distributions (Figs. 1(a), 1(b)), we obtain a strong longitudinal (out-of-plane) electric field component (E_z^2). Based on the intensity line profiles (Fig. 1(c)), the ratio between the longitudinal component E_z^2 and the transverse component ($E_x^2 + E_y^2$) is about 0.55:0.45. According to the calculated field distributions (Figs. 1(a) and 1(b)), the different focus sizes for the longitudinal and

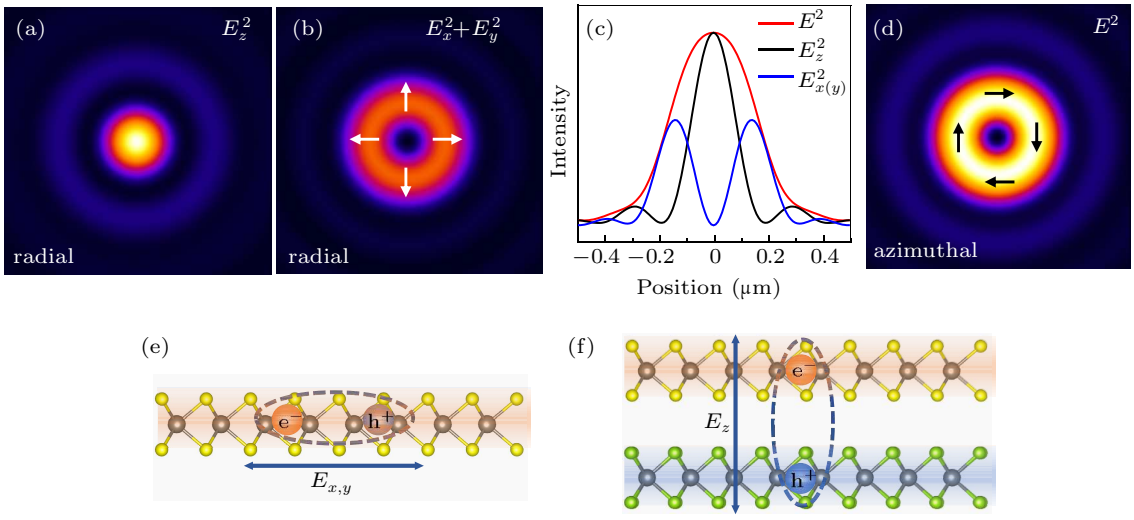


Fig. 1. Electric filed distributions at the focus of the polarized laser beam and the interaction with excitons in TMDCs. (a), (b) Calculated out-of-plane (E_z^2) and in-plane ($E_x^2 + E_y^2$) electric filed distributions at the focus of the radially polarized laser beam (532 nm) with an oil objective (NA = 1.4) and the corresponding (c) intensity profiles for the out-of-plane, in-plane and total electric field. (d) Calculated total electric field distributions at the focus of the azimuthally polarized laser beam, which is exclusively in-plane polarized ($E^2 = E_x^2 + E_y^2$). The image sizes are 1 μm × 1 μm. The arrows in (b) and (d) indicate the different in-plane polarizations. (e), (f) Illustrations of interaction of the electric field with the intralayer exciton in TMDCs atomic layers and the interlayer exciton in heterostructures, under the simple consideration of electric dipole.

azimuthal components result in an integrated area ratio of about 0.42:0.58. For an azimuthally polarized laser beam, the calculated electric field distribution shows only in-plane transverse electric field (Fig. 1(d)). Although the in-plane electric filed distributions in Figs. 1(b) and 1(d) show the same patterns, the polarizations are totally different due to the nature of the radial and azimuthal polarizations, as indicated by the arrows. With these distinct in-plane and out-of-plane electric field distributions, we can manipulate the different excitation configurations in TMDCs atomic layers and heterostructures. The intralayer exciton in TMDCs would have electron and hole located within the same layer (Fig. 1(e)), while the interlayer exciton with electron and hole located in different layers would form in TMDCs heterostructures (Fig. 1(f)).

3. Results and discussion

We first investigate the polarized PL spectroscopy of WS_2 atomic layers with different thicknesses using radially and azimuthally polarized laser beams. Figure 2(a) shows the optical image of the WS_2 flakes. From the optical contrast, we can distinguish the areas with different layer numbers from 1L to 4L, which are separated by the dashed lines. The layer numbers were further confirmed by Raman spectroscopy [41] (supporting information Fig. S2(a)).

Figure 2(b) shows the polarized PL spectra of the sample with different layer thicknesses. For the same flake, the spectra were auto-scaled, and the spectrum with higher intensity (red line) was collected under the excitation of the azimuthally polarized laser. Generally, there would be three PL characteristic peaks in few-layer WS_2, namely, A-, B-exciton emission peaks due to the spin–orbit coupling and the indirect bandgap emission (indirect exciton) peak.[42] The photon energy of B-exciton in 1L to 4L WS_2 is in the range of 2.34 eV–2.38 eV, which is greater than the single-photon energy of the 532 nm (2.33 eV) laser used in our experiments. Therefore, in this work, we only investigated the A-exciton and the indirect exciton related PL emission peaks.

To analyze the polarized spectra, we plotted the PL intensity and PL peak position from different layers in Figs. 2(c) and 2(d). As expected, for both laser modes, we clearly observe the PL intensity increase by orders of magnitude when the thickness of WS_2 changes from a few layers to monolayer, as a result of an indirect to direct bandgap transition. On the other hand, starting from bilayer, the indirect band transition emission outperforms the A-exciton emission with increasing layer number. As shown in Fig. 2(c), for all cases, the PL intensities of A-exciton and indirect bandgap peaks recorded under azimuthally polarized laser beam are stronger than those under radially polarized beam, which agrees with the strong in-plane component anisotropy in 2D TMDCs layers.[32] The peak energy of A-exciton shows a small shift from 2.01 eV (616.9 nm) of monolayer to 1.96 eV (632.6 nm) of bilayer, and the value has almost no changes with layer number increasing from 2L to 4L. While the peak energy of the indirect band transition gradually redshifts from 1.77 eV (700.5 nm), 1.59 eV (779.8 nm), to 1.52 eV (815.7 nm), when the thickness of the layer changes from 2L to 4L. These observations are consistent with the results obtained under the excitation of linear polarized lasers.[43] Regarding to the in-plane and out-of-plane

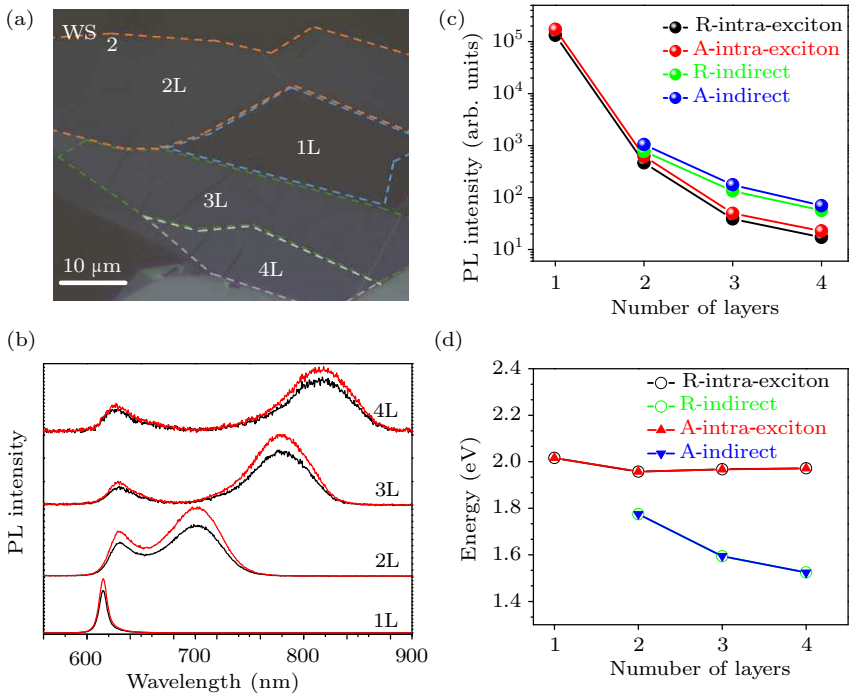


Fig. 2. Layers number dependent PL spectroscopy of WS_2 excited by the radially and azimuthally polarized laser beams. (a) Optical microscopy image of the WS_2 flakes prepared by the mechanical exfoliation from bulk crystal. (b) PL spectra of the 1L-, 2L-, 3L-, and 4L-WS_2 excited by both polarization modes. Spectra in red and black were taken with azimuthal and radial modes, respectively. (c), (d) Layer thickness dependent PL intensity and peak energy.

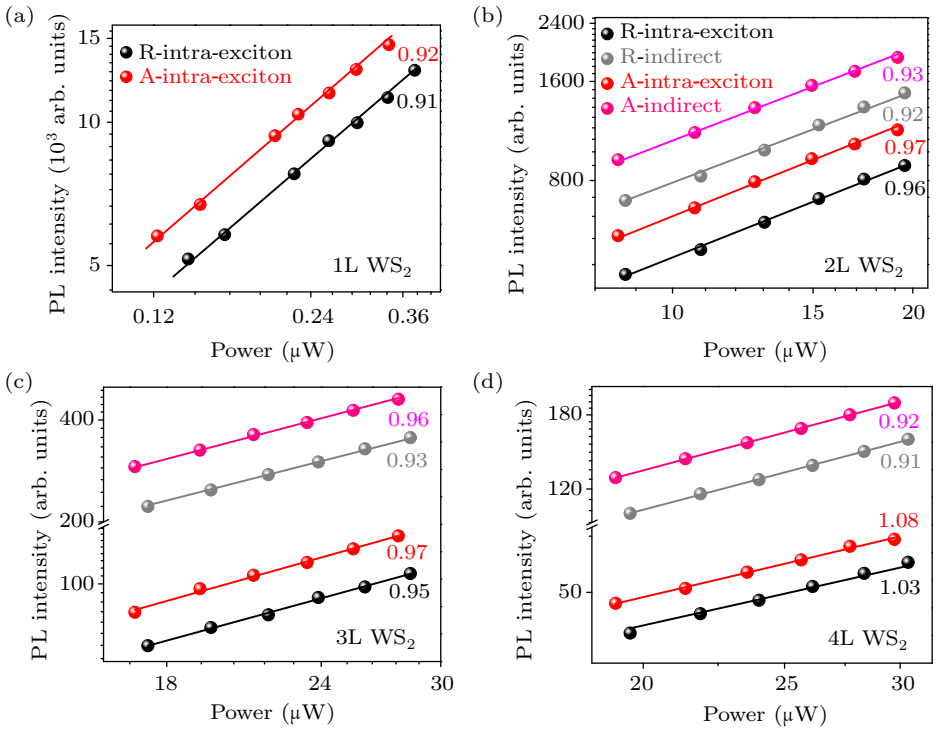


Fig. 3. Excitation power dependent PL spectroscopy of WS_2. (a)–(d) PL intensity for intralayer-exciton and indirect band gap transition from (a) 1L-, (b) 2L-, (c) 3L-, and (d) 4L-WS_2 atomic layers as a function of excitation power, under the excitation of both radially and azimuthally polarized laser beams. The solid lines show the linear fitting of the data on a double logarithmic scale, and the slopes of the fitting are shown as well.

polarization effect, we observe the same emission energy of excitons and indirect bandgap transition under the radial and azimuthal modes in our experiments (Fig. 2(d)), indicating the same excitonic origin of the PL emission. Furthermore, according to the normalized spectra (supporting information Fig. S3), we found almost identical spectral profiles under these two polarization excitations, which suggests that the A-exciton and indirect exciton emissions follow the same optical excitation configurations with effective electric dipole moments, mainly the in-plane component.

In order to compare the PL behaviors in a larger optical excitation power range with the different polarizations, we performed excitation power-dependent PL of 1L–4L WS_2 under the radial and azimuthal polarization modes (supporting information Fig. S4). All spectra were fitted to determine the peak position and peak intensity. The corresponding PL intensities as a function of the excitation power are shown in Fig. 3. For 2L–4L WS_2, both A-exciton and indirect exciton peaks are compared. With the linear fitting of the experimental data on a double logarithmic scale, we find that all the slopes are close to one, indicating the linear relation of the excitation law for intralayer exciton and indirect band transition. With the fitting data, we can accurately compare the PL intensity for the same excitation power. The ratio between PL intensities recorded with azimuthal and radial modes is about 1.3 at 20 μW. Within the excitation power range, we find the same polarization dependent tendency of intralayer and indirect exciton with these two laser modes.

It should be noted that all the spectra are the raw data recorded with the polarization modes, without the correction for the pure out-of-plane component in radial mode (Fig. 1(b)). However, considerable intensity is observed from the out-of-plane component, even excluded the contribution from the in-plane electric field from the radially polarized laser mode. This could be due to a small discrepancy between the theoretical calculated field distribution and the experimental conditions, and on the other hand the consideration of the orbital configuration in *xyz* three directions. The orbital of A-exciton consists mainly of $d_{x^2-y^2}$, d_{xy}, d_z^2 orbitals from W atom and a few p orbitals from S atom. For the optical excitation selection rules, the orbital distribution and overlaps need also to be considered,[44,45] although the electric dipole of intralayer exciton is mainly in-plane.

We also investigated the polarization dependent PL spectra in WSe_2 atomic layers. Similar as for the WS_2 samples, the thickness of different areas can be determined by the optical contrast (Fig. 4(a)) and further confirmed by the layer number dependent Raman spectroscopy[41] (supporting information Fig. S2(b)). Figure 4(b) shows the PL spectra of WSe_2 with different layer thicknesses under radial and azimuthal modes. We can observe the A-exciton and the indirect exciton for 2L–4L WSe_2. The position of the indirect transition peak red-shifts gradually from 789.8 nm (1.57 eV), 832.2 nm (1.49 eV) to 855 nm (1.45 eV) when the layer number increases from 2L to 4L, while the A-exciton peaks show only a small shift from 760.7 nm (1.63 eV) to 770.2 nm (1.61 eV).

We observed almost identical spectral profiles of A-exciton and indirect band transitions under these two different polarization excitations (supporting information Fig. S5), indicating the same electric dipole excitation configuration for A-exciton and indirect exciton in WSe_2. Power-dependent PL spectra were also collected under radial and azimuthal modes (supporting information Fig. S6). Figures 4(c) and 4(d) show the A-exciton and indirect band transition emission peak intensities (after Gaussian fitting) as a function of the excitation power for 1L- and 2L-WSe_2 atomic layers, respectively. We find a linear relation of the excitation law for intralayer exciton and indirect band transition and the emission intensity of WSe_2 with azimuthal mode is stronger than that with radial mode, consistent with the observation in WS_2 layers. Similar excitation power dependent tendency was observed for 3L- and 4L-WSe_2 atomic layers (supporting information Fig. S7).

Compared to the intralayer excitons, interlayer excitons formed by the combination of electrons in one layer and holes in the other layer, exist an electric dipole moment in the vertical (out-of-plane) direction. Therefore, we expect different spectral responses for intra- and inter-layer excitons under these two different polarization modes. Given this, bilayer WS_2/WSe_2 heterostructures were prepared and their optical polarizations were investigated. Figure 5(a) shows the optical images of the heterostructure, the area of which is marked with dashed lines. The polarized spectra of the heterostructure under both laser polarization modes are shown in Fig. 5(b). We observe three peaks appearing at 636.9 nm, 759.4 nm, and 834.5 nm, which can be ascribed to WS_2, WSe_2 in heterostructure and the interlayer exciton from WS_2/WSe_2 (Fig. 5(e)). Compared to the A-exciton emission peak from pure WS_2 and WSe_2 monolayers (dashed lines in Fig. 5(b)), the observed dominating emission peaks in the WS_2/WSe_2 heterostructure all locate at lower photon energy. As shown in the fitting of the spectra (supporting information Fig. S8), besides the strong PL emission with red-shifted photon energy, weak PL emissions maintain at the peak positions of the pure monolayers. It suggests that the peaks probably originate from trions of WS_2 and WSe_2 with the binding energy of about 40 meV, which are formed during the stacking of pure monolayers.[46,47] From the absolute emission intensity, spectra taken with azimuthal mode still are stronger than those with radial mode. For comparison, we normalized the spectra (Fig. 5(c)). While the peaks from WS_2 and WSe_2 are almost identical after the normalization, the interlayer exciton peak is obviously stronger under the excitation of the radial mode, as indicated by the black lines in Fig. 5(d). Based on the measurements, with respect to the intralayer exciton, we can estimate that the ratio between the out-of-plane and in-plane components of interlay exciton is about 1.35 (Fig. 5(d)). It should be noted that the local morphology and the stacking angle of the heterostructure may also affect the experimentally determination of the ratio of the in-plane and out-of-plane optical interlayer exciton dipole moments. Nevertheless, with the use of radial and azimuthal laser modes, we can clearly demonstrate the different in-plane and out-of-plane polarizations of intralayer and interlayer excitons.

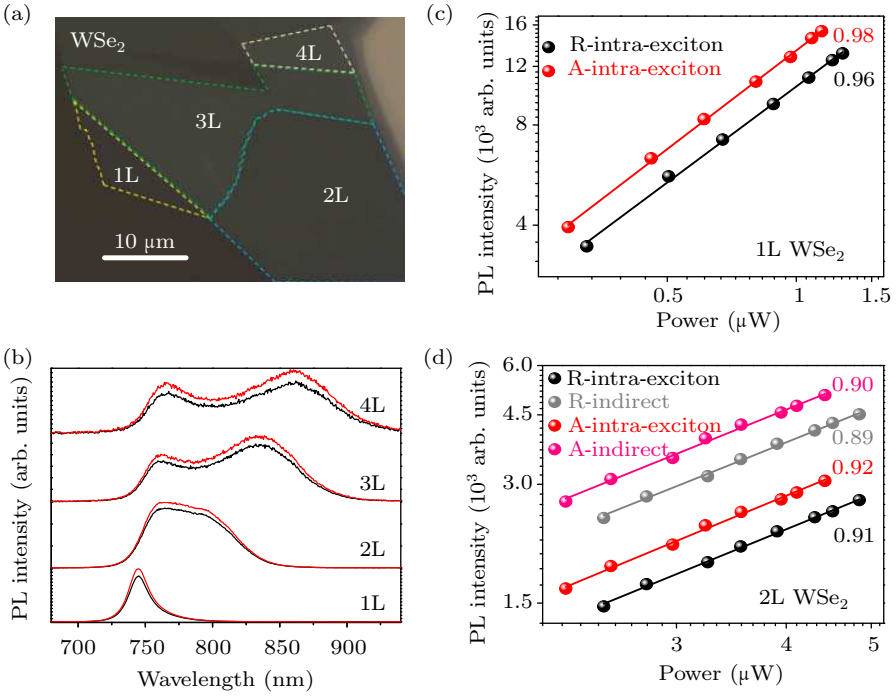


Fig. 4. Layers number and excitation power dependent PL spectroscopy of WSe_2 excited by the radially and azimuthally polarized laser beams. (a) Optical microscopy image of the WSe_2 flakes. (b) PL spectra of the 1L-, 2L-, 3L-, and 4L-WSe_2 excited by both azimuthal (red) and radial (black) modes. Excitation power dependent PL intensity (double logarithmic scale) for intralayer-exciton and indirect band gap transition from (c) 1L-, and (d) 2L-WSe_2 atomic layers. The solid lines are the fittings for the data.

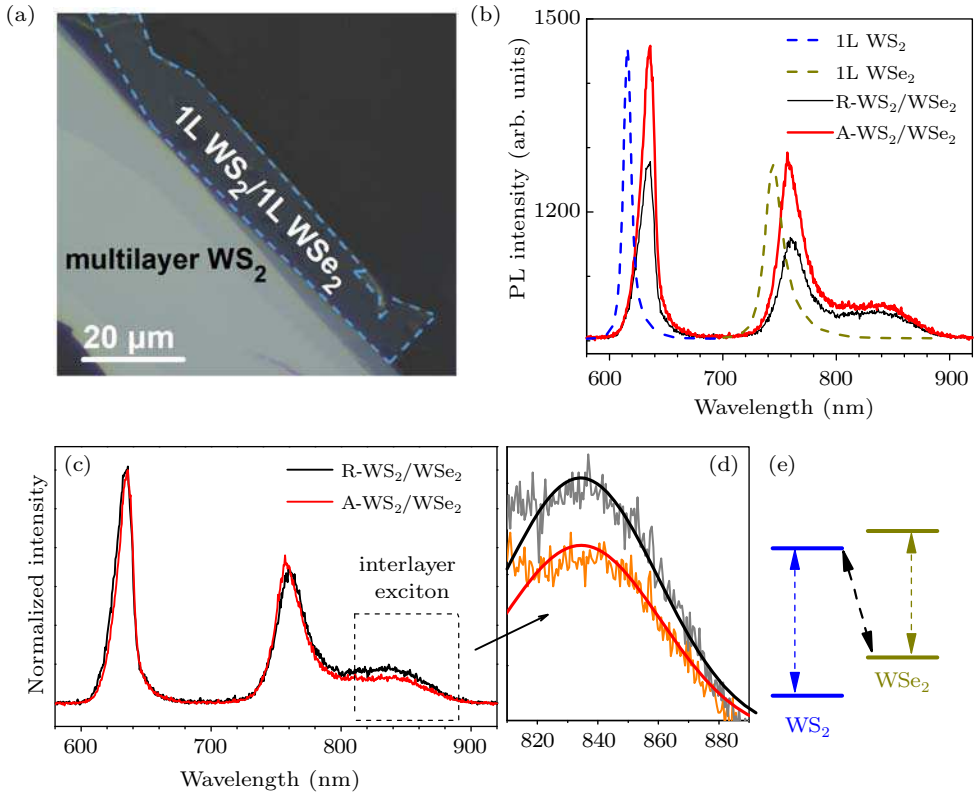


Fig. 5. Polarized PL properties of interlayer excitons in a WS_2/WSe_2 heterostructure. (a) Optical microscope image of the heterostructure consisting of monolayers of WS_2 and WSe_2. (b) PL spectra taken from the heterostructure area excited by radially and azimuthally polarized laser beams. PL spectra from monolayer WS_2 and WSe_2 are shown as dashed lines for comparison. (c), (d) Normalized polarized spectra and the zoom in at the spectral range for the interlayer exciton (dashed black rectangular). (e) Illustration of the WS_2/WSe_2 band alignment, the black dashed arrow indicates interlayer exciton transition.

4. Conclusion

In summary, the intralayer and indirect exciton in WS_2 and WSe_2 atomic layers and interlayer exciton in WS_2/WSe_2 heterostructures were investigated with radially and azimuthally polarized laser beams. With excitation power and layer thickness dependent spectroscopy, we conclude that the intralayer exciton and indirect band transition have the same in-plane and out-of-plane polarization behavior. The interlayer exciton in WS_2/WSe_2 heterostructures shows stronger out-of-plane polarization, due to the formed vertical electric dipole moment of the exciton. Our study not only contributes to the fundamental understanding of the polarization of intralayer, interlayer, and indirect exciton, but also provides important information for exitonic optoelectronic device applications.

References

[1] Wang Q H, Kalantar-Zadeh K, Kis A, Coleman J N and Strano M S 2012 *Nat. Nanotechnol.* **7** 699

[2] Xu X D, Yao W, Xiao D and Heinz T F 2014 *Nat. Phys.* **10** 343

[3] Sun Z P, Martinez A and Wang F 2016 *Nat. Photon.* **10** 227

[4] Wang J, Han J Y, Chen X Q and Wang X R 2019 *Infomat.* **1** 33

[5] Ge C H, Li H L, Zhu X L and Pan A L 2017 *Chin. Phys. B* **26** 034208

[6] Cheng Q L, Pang J B, Sun D H, Wang J G, Zhang S, Liu F, Chen Y K, Yang R Q, Liang N, Lu X H, Ji Y C, Wang J, Zhang C C, Sang Y H, Liu H and Zhou W J 2020 *Infomat.* **2** 656

[7] Cheng Y, Huang C, Hong H, Zhao Z X and Liu K H 2019 *Chin. Phys. B* **28** 107304

[8] Qin M S, Zhu P F, Ye X G, Xu W Z, Song Z H, Liang J, Liu K H and Liao Z M 2021 *Chin. Phys. Lett.* **38** 017301

[9] Chernikov A, Berkelbach T C, Hill H M, Rigosi A, Li Y L, Aslan O B, Reichman D R, Hybertsen M S and Heinz T F 2014 *Phys. Rev. Lett.* **113** 076802

[10] Ross J S, Klement P, Jones A M, Ghimire N J, Yan J Q, Mandrus D G, Taniguchi T, Watanabe K, Kitamura K, Yao W, Cobden D H and Xu X D 2014 *Nat. Nanotechnol.* **9** 268

[11] Ciarrocchi A, Unuchek D, Avsar A, Watanabe K, Taniguchi T and Kis A 2018 *Nat. Photon.* **13** 131

[12] Zheng W H, Jiang Y, Hu X L, Li H L, Zeng Z X S, Wang X and Pan A L 2018 *Adv. Opt. Mater.* **6** 1800420

[13] Ma X L, Zhang R J, An C H, Wu S, Hu X D and Liu J 2019 *Chin. Phys. B* **28** 037803

[14] Zeng Z X S, Wang X and Pan A L 2020 *Acta Phys. Sin.* **69** 184210 (in Chinese)

[15] Mak K F, Lee C, Hone J, Shan J and Heinz T F 2010 *Phys. Rev. Lett.* **105** 136805

[16] Ramasubramaniam A, Naveh D and Towe E 2011 *Phys. Rev. B* **84** 205325

[17] Zeng F, Zhang W B and Tang B Y 2015 *Chin. Phys. B* **24** 097103

[18] Cheng Y, Huang C, Hong H, Zhao Z X and Liu K H 2019 *Chin. Phys. B* **28** 107304

[19] Paradisanos I, Shree S, George A, Leisgang N, Robert C, Watanabe K, Taniguchi T, Warburton R J, Turchanin A, Marie X, Gerber I C and Urbaszek B 2020 *Nat. Commun.* **11** 2391

[20] Geim A K and Grigorieva I V 2013 *Nature* **499** 419

[21] Liu Y, Weiss N O, Duan X D, Cheng H C, Huang Y and Duan X F 2016 *Nat. Rev. Mater.* **1** 16042

[22] Zhang D L, Liu Y, He M, Zhang A, Chen S L, Tong Q J, Huang L Y, Zhou Z Y, Zheng W H, Chen M X, Braun K, Meixner A J, Wang X and Pan A L 2020 *Nat. Commun.* **11** 4442

[23] Li J H, Bing D, Wu Z, Wu Z T, Wu G Q, Bai J, Du R X and Qi Z Q 2020 *Chin. Phys. B* **29** 017802

[24] He Y F, Wang L X, Xiao Z X, Lv Y W, Liao L and Jiang C Z 2020 *Chin. Phys. Lett.* **37** 088502
[25] Chang Z, Yuan K P, Sun Z H, Zhang X L, Gao Y F, Gong X J and Tang D W 2021 *Chin. Phys. B* **30** 034401
[26] Li L H, Zheng W H, Ma C, Zhao H P, Jiang F, Ouyang Y, Zheng B Y, Fu X W, Fan P, Zheng M, Li Y, Xiao Y, Cao W P, Jiang Y, Zhu X L, Zhuang X J and Pan A L 2020 *Nano Lett.* **20** 3361
[27] Miller B, Steinhoff A, Pano B, Klein J, Jahnke F, Holleitner A and Wurstbauer U 2017 *Nano Lett.* **17** 5229
[28] Jauregui L A, Joe A Y, Pistunova K, Wild D S, High A A, Zhou Y, Scuri G, De Greve K, Sushko A, Yu C-H, Taniguchi T, Watanabe K, Needleman D J, Lukin M D, Park H and Kim P 2019 *Science* **366** 870
[29] Unuchek D, Ciarrocchi A, Avsar A, Watanabe K, Taniguchi T and Kis A 2018 *Nature* **560** 340
[30] Liu Y D, Dini K, Tan Q H, Liew T, Novoselov K S and Gao W B 2020 *Sci. Adv.* **6** 1830
[31] Li W J, Lu X, Dubey S, Devenica L and Srivastava A 2020 *Nat. Mater.* **19** 624
[32] Funke S, Miller B, Parzinger E, Thiesen P, Holleitner A W and Wurstbauer U 2016 *J. Phys. Condens. Matter* **28** 385301
[33] Zhan Q W 2009 *Adv. Opt. Photon.* **1** 1
[34] Züchner T, Failla A V and Meixner A J 2011 *Angew. Chem. Int. Ed.* **50** 5274
[35] Novotny L, Beversluis M R, Youngworth K S and Brown T G 2001 *Phys. Rev. Lett.* **86** 5251
[36] Wang X, Broch K, Scholz R, Schreiber F, Meixner A J and Zhang D 2014 *J. Phys. Chem. Lett.* **5** 1048
[37] Wang X, Zhuang X J, Wackenhut F, Li Y Y, Pan A and Meixner A J 2016 *Laser Photonics Rev.* **10** 835
[38] Wang X, Zeng Z X S, Zhuang X J, Wackenhut F, Pan A L and Meixner A J 2017 *Opt. Lett.* **42** 2623
[39] Bautista G, Huttunen M J, Kontio J M, Simonen J and Kauranen M 2013 *Opt. Express* **21** 21918
[40] Castellanos-Gomez A, Buscema M, Molenaar R, Singh V, Janssen L, van der Zant H S J and Steele G A 2014 *2D Materials* **1** 011002
[41] Zhao W J, Ghorannevis Z, Amara K K, Pang J R, Toh M, Zhang X, Kloc C, Tan P H and Eda G 2013 *Nanoscale* **5** 9677
[42] Zhao W J, Ribeiro R M, Toh M, Carvalho A, Kloc C, Castro Neto A H C and Eda G 2013 *Nano Lett.* **13** 5627
[43] Zeng H, Liu G B, Dai J F, Yan Y J, Zhu B, He R, Xie L, Xu S J, Chen X H, Yao W and Cui X D 2013 *Sci. Rep.* **3** 1608
[44] Yu H, Liu G B and Yao W 2018 *2D Material* **5** 035021
[45] Sun S B, Dang J C, Xie X, Yu Y, Yang L L, Xiao S, Wu S Y, Peng K, Song F L, Wang Y N, Yang J N, Qian C J, Zuo Z C and Xu X L 2020 *Chin. Phys. Lett.* **37** 087801
[46] Yu J, Kuang X F, Zhong J H, Cao L K, Zeng C, Ding J N, Cong C X, Wang S H, Dai P F, Yue X F, Liu Z W and Liu Y P 2020 *Opt. Express* **28** 13260
[47] Ye T, Li J Z and Li D H 2019 *Small* **15** 1902424